 

# A Numerical Study of High Resolution Latent Image Generation by Laser Beam Exposure

*Yoshio Watanabe, Hiroyuki Kawamoto, Hisashi Shoji,*
*Hirokatsu Suzuki, and Yumiko Kishi*
*Ricoh Co. Ltd., Yokohama, Japan*

## Abstract

In order to study the latent image generation process including the characteristics of laser beam and photoreceptor, a numerical method which solves the three dimensional time dependent coupled system of the transport equations for charges and the Poisson equation for electrostatic field is proposed. Combining the simulation with electrostatic field computation in development region, the strength and the extent of spreading of the electrostatic field due to the latent image is analyzed. The image of isolated 1 dot exposure shows larger spreading, while that of 1 by 1 dot shows weaker electrostatic-field strength. The dependence of the spreading on the beam radius indicates that the repulsion of charge due to space-charge effect becomes significant as the beam diameter decreases. The numerical results are compared with the experimental ones of a test-bed for the high-resolution development, and show the excellent correlation with the experimental developed images.

## Introduction

In electrophotography, the high-resolution latent image generation is the first step in order to achieve the high quality printing. As pointed by Williams[1], the latent image may be degraded by the lateral electrostatic field due to the neutralization of the surface charge with the charge generated in photoreceptor, and also by the Coulomb self-repulsion of the charge in the photoreceptor. In printers and digital copiers, the small dots are formed by laser beam exposure, which generates much denser charge in the photoreceptor than the halogen lump does. As the dot size becomes smaller towards the high quality image, the Coulomb self-repulsion becomes much severer, because the repulsive force is proportional to the square of the charge density.

Several research[2,3] has been made to investigate the latent image generation for the actual dot image using the photo-induced discharge curve(PIDC) obtained from solid image. The simulation system adopting the PIDC requires small computation to predict the developed image even for the actual complex pattern. From the material research viewpoint, the photodischarge in photoreceptors are analyzed considering such material properties as mobility and quantum efficiency[4,5]. Extending Schaffert's[6] and Scharfe's[7] studies, the electrostatic field in the development region has been studied extensively[8,9].

In order to study the effect of small beam spot size on the printing quality further, it is necessary to analyze the behavior of charge carrier in detail. In this paper, we present a new stable and fast numerical method that solves the charge carrier transport equations as well as the Poisson equation of electrostatic field in photoreceptors. Our numerical model includes the nonlinear Coulomb self-repulsion effect of charges along with the generation and recombination of charges. Combining the computation of the laser beam exposure and the electrostatic field in the development region, a three dimensional latent image simulator is developed. We simulate the latent images for solid, isolated 1 dot and 1 by 1 dot exposure, and compare with the experiments of a test-bed for the high-resolution development.

## Simulation Model of the Latent Image Generation

The simulation system consists of three steps: the first is the calculation of Gaussian laser beam exposure, the second is the simulation of the charge transport process in photoreceptor and the third is the electrostatic computa-tion in the development region. The first and the third steps are solved using the well-known methods.

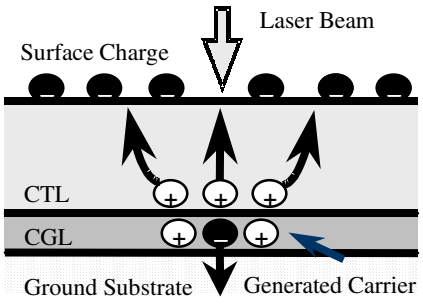


*Figure 1. Schematic diagram of charge generation and transport in OPC*

The second step describes the carrier generation in CGL and the transport in CTL under the electrostatic field due to the surface charge on OPC and charge in OPC, as shown in figure 1. The mathematical representation for the above process is,

$$\frac{\partial n_p}{\partial t} + div\left(\mu_p \mathbf{E} n_p\right) = \Gamma - R\, n_p\, n_n \quad (1)$$

$$\frac{\partial n_n}{\partial t} + div\left(-\mu_n \mathbf{E} n_n\right) = \Gamma - R\, n_p\, n_n \quad (2)$$

$$div\left(\varepsilon \mathbf{E}\right) = e\left(n_p - n_n\right) \quad (3)$$

$$where\ \mathbf{E} = -grad\left(\phi\right). \quad (4)$$

Here, $n$, μ, E, Γ, $R$, ε, $e$, ϕ are the number density of charge, the mobility of OPC, the electric field, the charge generation rate, the charge recombination rate, the dielectric constant, the elementary electric charge and the electric potential, respectively. The subscript $p$ and $n$ indicate the quantities for the positive and negative charge, respectively.

The CGL layer is assumed to be optically thin, which allows the charge generation rate Γ to be written as,

$$\Gamma = \beta \cdot \eta \cdot F \big/ \left(d \cdot h\nu\right), \quad (5)$$

where $\beta$, $\eta$, $F$, $d$ and $h\nu$ are the absorption and quantum efficiency of CGL, the incident laser beam flux, the thickness of CGL and the energy of a photon, respectively.

The recombination terms in equations (1) and (2) are introduced in order to explain the experiment for the solid image described in the following section, which shows the decrease of total charge generated in CGL when the incident light becomes stronger. The absorption efficiency β represents the absorbed photons in CGL for the total incident photons on the CGL. The recombination rate $R$ and absorption efficiency β is determined experimentally using the results for solid image.

## Numerical Method

The finite difference method is used to solve the above coupled equations (1), (2) and (3). We adopt the time-forward difference for the time derivatives and the upwind difference for the advection terms in equations (1) and (2). All terms except the time derivatives are evaluated implicitly; namely evaluated at the (n+1)th step, where n is the time step that indicates known status and the (n+1)th is the future unknown step. The final form is written as:

$$\frac{n_p^{n+1} - n_p^{n}}{\delta t} = -\left[div\left(\mu_p \mathbf{E} n_p\right)\right]^{n+1} + \Gamma^{n+1} - R\, n_p^{n+1} n_n^{n+1} \quad (6)$$

$$\frac{n_n^{n+1} - n_n^{n}}{\delta t} = -\left[div\left(-\mu_n \mathbf{E} n_n\right)\right]^{n+1} + \Gamma^{n+1} - R\, n_p^{n+1} n_n^{n+1} \quad (7)$$

$$div\left(\varepsilon \cdot grad\, \phi^{n+1}\right) = -e\left(n_p^{n+1} - n_n^{n+1}\right), \quad (8)$$

where $\delta t$ is the time interval between the successive steps. The above nonlinear algebraic equations (6), (7) and (8) are solved using the "double iteration" method. The first outer iteration loop consists of successive substitution over the whole three equations. The inner iteration loop uses successive over-relaxation method to get the temporal solution for each equation. In the inner loop, all variables except the variable under consideration is assumed to be known by the preceding iteration steps. For example, successive over-relaxation focuses only on $n_p$ in equation (6), and other variables are assumed to be known.

The implicit scheme allows us the flexible time interval $\delta t$, because it is unconditionally stable. We adopt the very small time interval when the laser beam illuminates the CGL and the very high density charge is generated, while larger time interval is used to simulate the evolution of the charge cloud in CTL.

The numerical method is reasonably fast and requires less computer memories. The simulation mentioned in the next sections is performed using a PENTIUM II 233MHz processor with 64Mbytes.

## Numerical Results and Comparison with Test-Bed Experiments

### Spatial and Temporal Feature of the Simulation

As a typical example of the simulation, we give the numerical result for the 1200dpi isolated 1 dot latent image generation in figure 2, which shows the three dimensional view of charge density at 50μsec. The horizontal direction(x-direction) means the scanning direction of the laser beam, and the vertical one(y-direction) implies the perpendicular direction. The z-direction indicates the depth position. The laser beam is round shape with 0.21mW power and the spot size is 30μm. The 15 μm thick azo-compound OPC is used, and the surface is charged at –870V initially. The charge is transported as hole in CTL. The straight lines in the cross-sections indicate the $1/e^2$ beam size of the incident laser for the (y,z) plane and $1/e^2$ beam size plus the laser scanning length of 21.2μm for the (x,z) plane, respectively.

The evolution of the charge cloud in OPC is shown in figure 3, which suggests that the charge cloud has already expanded at 50μsec due to their Coulomb self-repulsion. The electric potential is distorted by the space charge effect, which makes the drift of the cloud slower.

### Solid Image and 1 by 1 line image

Figure 4 shows the surface potential for different beam sizes and powers by the simulations and the test-bed experiments averaged over the OPC surface. The result of 70μm beam size of solid image is used to adjust $\beta$. The experimental result of 30μm beam with 0.21mW power shows that the total charge generated in CGL depends on the beam size, which implies that the beam intensity affects the charge generation efficiency. As mentioned in the previous section, we introduce the recombination term and make $R$ fit to the data.

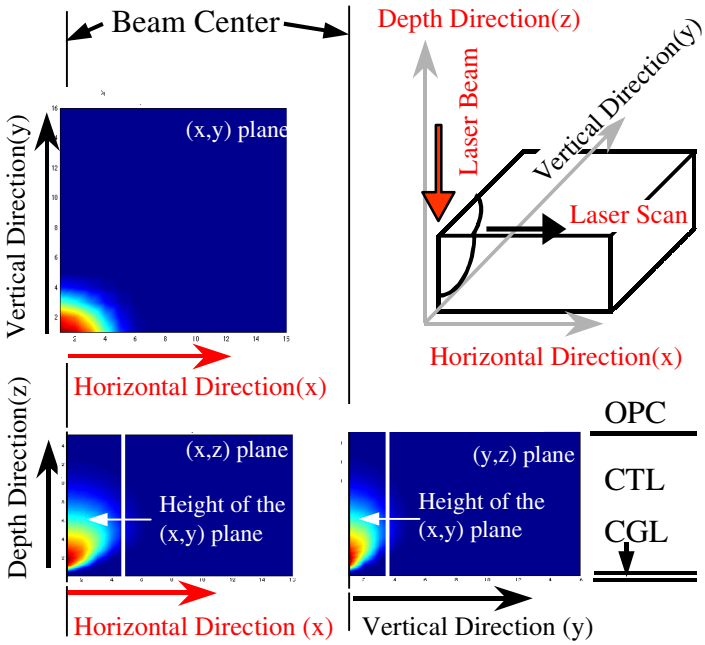


*Figure 2. Three dimensional view of charge density at 50µsec of the charge(hole) cloud. The laser beam spot size is 30µm and the OPC thickness is15µm. The straight line for the (y,z) plane indicates the $1/e^2$ beam size of the incident laser, and that for the (x,z) plane does the $1/e^2$ beam size plus the laser scanning length for 1 dot.*

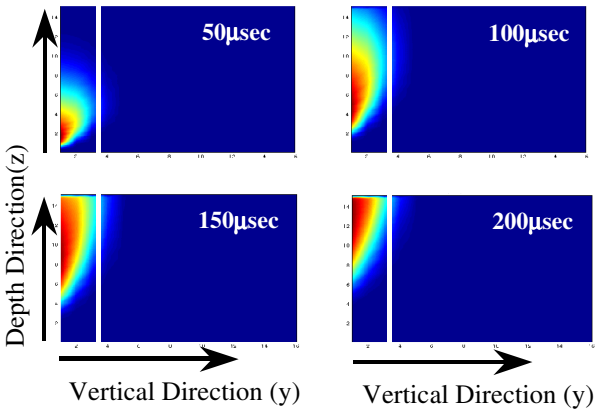


*Figure 3. The evolution of charge(hole) cloud. The figures show the cross-sections normal to horizontal direction(scanning direction).*

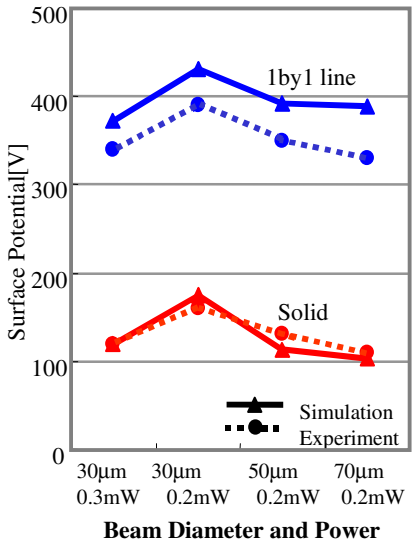


*Figure 4. Simulated and experimental average surface potential for different beam sizes and powers*

The numerical results for 1 by 1 line are about 30-50V greater than the experimental results. The reason of this discrepancy is due to the about 10% error of the total charge generation. However, the numerical simulation reproduces well the overall dependence of the surface potential on the beam size and the power, and is used to evaluate the latent image generation for various patterns.

**Isolated 1 dot image**

The isolated 1 dot latent image is simulated for 30µm and 50µm beam sizes and for 15µm and 28µm thick OPC. Figure 5 shows the numerical electric field and the laser beam intensity that is normalized to the maximum and minimum of the electric field. The abscissa indicates the horizontal or vertical position on the OPC. The developed images by the high-resolution test-bed experiments are also shown.

These results lead us to find the good correlation between the numerical results and experimental images, and the threshold dividing the image quality is about $4\times10^6$[V/m], which is marked in the figure. The figure also shows that the 30µm beam size makes the spreading of the latent image severer even for 15µm thick OPC as well as 28µm one. It comes from the Coulomb self-repulsion described in the previous section.

**1 by 1 dot image**

Figure 6 shows the numerical and experimental results for 1 by 1 dot image under the same condition of the isolated 1 dot results. While the 1 by 1 latent image can be developed by the lower electric field than that for the isolated 1 dot, the electric field of $4\times10^6$[V/m] is a rough threshold for the image quality. The spreading of the latent image is less than that of the isolated 1 dot, because the neighboring dots suppress the expansion of the charge cloud. On the other hand, the strength of the electric field is lower than that for the isolated 1 dot, because the edge effect decreases by the neighboring dots.

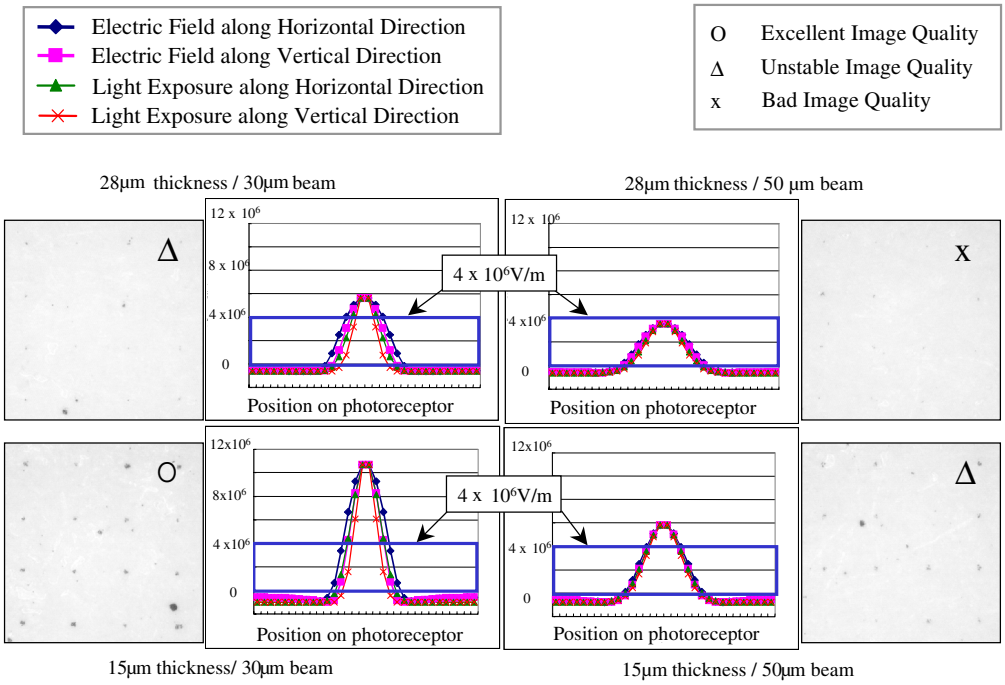


*Figure 5. Electric field strength and light exposure for isolated 1 dot with experimentally developed images*

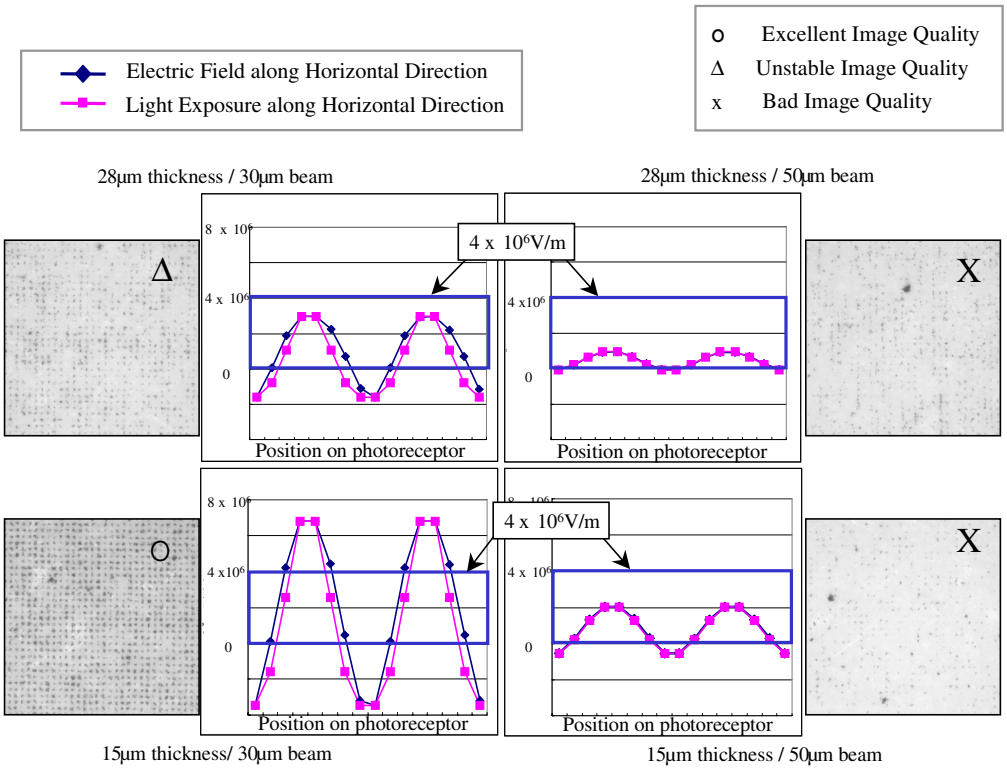


*Figure 6. Electric field strength and light exposure for 1 by 1 dot with experimentally developed images*

## Conclusion

In order to simulate the three dimensional latent image generation, a new numerical method is proposed adopting a "double iteration" method for the implicit finite difference equations for the charge transport equations and the Poisson equation for electrostatic field. The method is fast and stable, and requires less computer resources. The simulated latent image of isolated 1 dot exposure shows larger spreading and greater electrostatic field than that of 1 by 1 dot. The dependence of the spreading on the beam radius indicates that the repulsion of charge due to space-charge effect becomes significant as the beam diameter decreases.

The numerical results show the excellent correlation with the experimental images from a test-bed for the high-resolution development.

## References

1. E.M. Williams, The Physics and Technology of Xerographic Processes, Chap.2, John Wiley and Sons, Inc.(1984).
2. N. Kawamura and M. Itoh, Electrophotography, **26**, 364(1987).
3. T. Motoi, Konica Technical Report, **5**, 89(1992).
4. P.M. Borsenberger and D.S. Weiss, Organic Photoreceptors for Xerography, Chap.3, Marcel Dekker, Inc.(1998).
5. K. Oka and S. Fujiwara, Journal of the Imaging Society of Japan, **38**, 296(1999).
6. R.M. Shaffert, Electrophotography, 2nd ed., Focal Press (1975).
7. M. Scharfe, Electrophotography Principles and Optimization, Chap.4, Research Studies Press Ltd.(1984).
8. H. Imada, A. Hakamoto, T. Higashiguchi, H. Kiwaki and S. Takeuchi, Electrophotography, **32**, 253(1993).
9. T. Iwamatsu, T. Toyoshima, N. Azuma, Y. Mutou and Y. Nakajima, IS&T's NIP15: International Conference on Digital Printing Technologies, 732(1999).

## Biography

Yoshio Watanabe received his B.S. degree in Physics and Dr. degree in Astrophysics from Kyoto University in 1974 and 1984, respectively. After the work in the nuclear engineering area in Century Research Center, he joined Ricoh Co. Ltd. in 1985. He has been engaged in the numerical simulation of corona discharge, development process and latent image generation in electrophotography as well as the flow analysis in toner production technology.